Available online at www.sciencedirect.com

ScienceDirect

Progress in Natural Science: Materials International 24 (2014) 239–246

Progress in Natural Science Materials International

www.elsevier.com/locate/pnsmi
www.sciencedirect.com

Original Research

High-energy ion treatments of amorphous $As_{40}Se_{60}$ thin films for optical applications

Rashmi Chauhan[a,*], Arvind Tripathi[b], Krishna Kant Srivastava[c]

[a]Department of Physic, DAV College, CSJM University, Kanpur 208001, India
[b]Research Foundation for Education and Technology, Datia 475661, India
[c]Department of Physics, DBS College, CSJM University, Kanpur 208006, India

Received 21 December 2013; accepted 26 April 2014
Available online 27 May 2014

Abstract

The treatment of 100 MeV Ag swift-heavy ion (SHI) irradiation with five different fluences (3×10^{10}, 1×10^{11}, 3×10^{11}, 1×10^{12}, and 3×10^{12} ions/cm^2) was used to design optical and structural properties of amorphous (a-) $As_{40}Se_{60}$ chalcogenide thin films. Swanepoel method was applied on transmission measurements to determine the changes in optical bandgap, Tauc parameter and linear optical parameters, i.e., linear optical absorption, extinction coefficient and linear refractive index. Dispersion of the material was determined by Wemple–DiDomenico relation. Changes in nonlinear optical parameters of third-order optical susceptibility and nonlinear refractive index were determined using semi-empirical relations. Changes in surface morphology of the films were investigated using SEM observation, which indicated that fluence 3×10^{12} ions/cm^2 was upper threshold limit for these films for ion treatment. It is observed that optical bandgap reduces from 1.76 eV to 1.64 eV, and nonlinear refractive index increases from 1.31×10^{-10} [esu] to 1.74×10^{-10} [esu]. Linear refractive index initially increases from 2.80 to 3.52 (for fluence 3×10^{10} ions/cm^2) and then keeps decreasing. The observed changes in optical properties upon irradiation were explained in terms of structural rearrangements by Raman measurement. The study was compiled with the previous literature to propose SHI as an effective optical engineering technique to achieve desired changes according to the need of optical/photonic applications.

Keywords: Amorphous chalcogenide thin films; Ion irradiation; Linear and nonlinear optical properties; Swanepoel method; Semi-empirical relations; Raman measurements

1. Introduction

Ion irradiation is an effective technique to design material properties according to desired application. Energetic ions are divided into two categories, which are low energy ion (energy ranging from few tens of keV to hundreds of keV) and high energy ion (energy ranging from few tens of MeV to GeV). Low energy ion imparts energy to the material through elastic collision; hence nuclear energy loss (of the order of 10 keV/amu) is mainly responsible for material modification [1]. High energy ion, also known as swift-heavy ion (SHI), deposits energy to the target material through inelastic collision. In an inelastic collision, incident ion transfers energy to the electron cloud and the electron transfers energy to the lattice via electron–phonon interaction. Hence, in SHI irradiation, electronic energy loss (of the order of 1 MeV/amu) is mainly responsible for material modification [1]. Here, the interaction between SHI and target material causes structural disorder, defects and columnar amorphization in the material, which are responsible for the change in optical and optoelectronic properties of the material [1–4]. These changes depend on

*Corresponding author. Tel.: +91 933 633 9469.
E-mail addresses: chauhanrasmi@gmail.com (R. Chauhan), arvindtri@gmail.com (A. Tripathi), krishnakantsrivastava@hotmail.com (K.K. Srivastava).

Peer review under responsibility of Chinese Materials Research Society.

Production and hosting by Elsevier

http://dx.doi.org/10.1016/j.pnsc.2014.05.006
1002-0071/

the amount of electronic energy loss of swift-heavy ion, which further depends on energy and mass of the incident ion, target material and ion fluence. Hence, engineering of material properties is possible on the basis of above mentioned factors.

Amorphous chalcogenides are important optical materials, which have a wide range of ion-sensitivity. Hence, these materials are used to fabricate optical elements using ion irradiation [5,6]. In the present study, 100 MeV Ag ions are used for five different fluences (3×10^{10}, 1×10^{11}, 3×10^{11}, 1×10^{12}, and 3×10^{12} ions/cm^2) and target material is a-$As_{40}Se_{60}$ chalcogenide thin film. Choice of a-$As_{40}Se_{60}$ as target material is due to its wide use in photonic applications [7,8]. In an earlier study, we have published results for changes in linear optical absorption (α), optical bandgap (E_g) and static refractive index (n_0) of a-$As_{40}Se_{60}$ thin films under 100 MeV Ag ion irradiations [8], where α and n_0 were determined using Lambert–Beer's law and Dimitrov–Sakka relations [9] respectively. In the present study, we have determined wavelength dependent linear optical parameters using Swanepoel method [10]. In addition, nonlinear refractive index was determined using Tichy [11] relation. Third-order optical nonlinearity was also determined using Miller rule [12,13].

2. Experimental

Bulk $As_{40}Se_{60}$ glass was prepared by conventional melt quenching technique. Corresponding elements (As and Se with purity 99.99%) were weighed according to their atomic percentages, sealed in quartz ampoules at base pressure of 1.33×10^{-3} Pa (10^{-5} Torr), and then kept inside a furnace to heat up to 940 °C at the heating rate of 3–4 °C/min. To ensure the achieved melt to be homogeneous, these ampoules were frequently rocked for 10 h at 940 °C, and then quenched in ice water. To prepare amorphous thin films of glassy alloy, thermal evaporation technique was used. Film deposition was carried out onto the cleaned glass substrates at the deposition-rate of 1–5 nm/s at room temperature inside a coating system (HIND-HIVAC Model 12A 4DT) at the base pressure of 1.33×10^{-4} Pa (10^{-6} Torr). Amorphous natures of the bulk sample and thin films were verified using X-ray diffraction measurements (Thermo Electron Corporation, Model ARL X'TRA) with Cu Kα radiation at the scan rate of 3°/min. 100 MeV Ag SHI irradiation was performed using a 15 UD pelletron tandem accelerator at IUAC, New Delhi for five different fluences (3×10^{10}, 1×10^{11}, 3×10^{11}, 1×10^{12}, and 3×10^{12} ions/cm^2). The irradiated area of thin films was 1 cm^2. Surface morphology and stoichiometry of the films were determined using a Scanning Electron Microscope (INCA PentaFET3). The optical transmissions for normal incidence of thin films were measured using a double beam UV/vis computerized spectrophotometer (Hitachi, Model U-3300) in the wavelength range of 300–900 nm. The film thicknesses were measured using a mechanical thickness profilometer (Tencore Instrument, Model Alpha Step 100). For structural analysis, micro-Raman measurements were performed on a spectrometer (Renishaw In Via Raman Microscope) using a 515.4 nm Argon ion laser with a power density 5 mW/cm^2 at room temperature.

3. Results and discussion

3.1. XRD, EDAX and SEM measurements

Fig. 1 shows XRD patterns of pristine and irradiated thin film (fluence 3×10^{12} ions/cm^2). The absence of any sharp peak implies that films retain amorphous nature under SHI irradiation. The presence of the hump in pristine film is an indication of small to medium range order in amorphous thin film. SHI irradiation causes disappearance of the hump. This nature is an indication of the increase in disorder in the film, which is further explained by Raman and UV/vis measurements.

Fig. 2 shows EDAX measurements at different spots along with the diameter in thin films. EDAX picture shows the peaks for As and Se contents along with some additional peaks appeared due to gold coating on the film. The composition derived from the EDAX image of thin film is $As_{40.8}Se_{59.2}$. Hence, little over-stoichiometry in Arsenic (As) and sub-stoichiometry of Selenium (Se) is observed due to the volatile nature of Selenium.

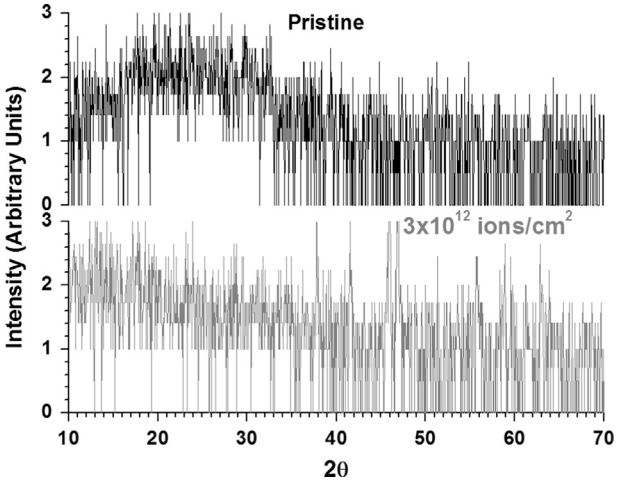

Fig. 1. XRD patterns of pristine and irradiated (3×10^{12} ions/cm^2) thin film.

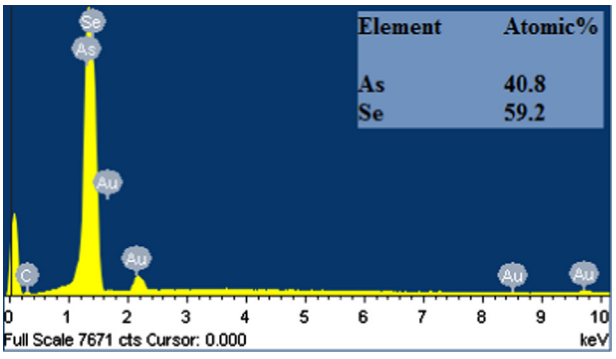

Fig. 2. EDAX spectrum of pristine thin film.

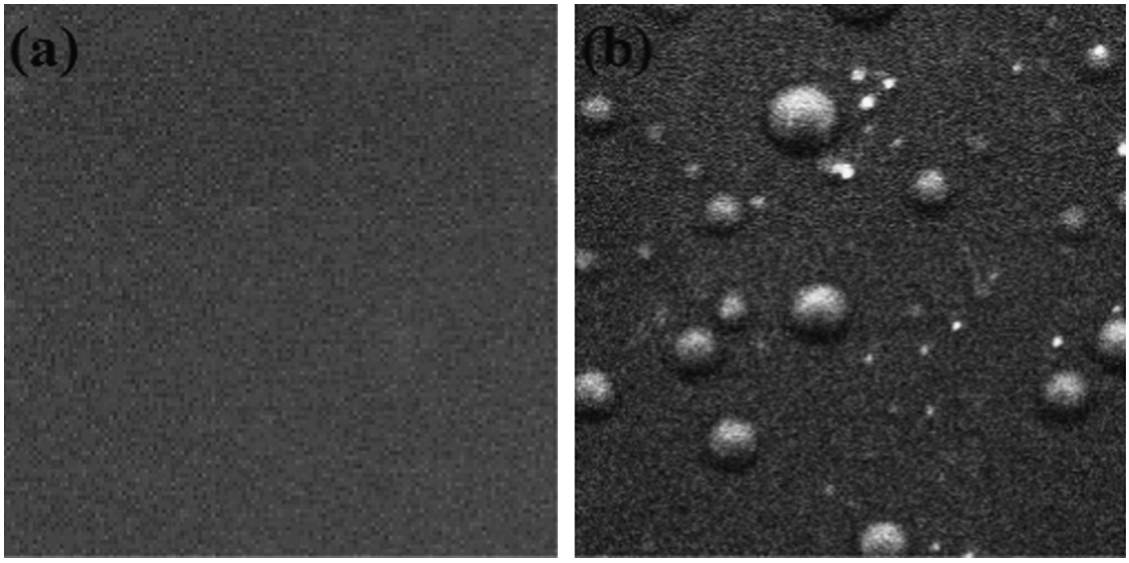

Fig. 3. SEM images of (a) pristine thin film at 10 μm and (b) irradiated thin film (3×10^{12} ions/cm^2) at 100 μm.

Fig. 3 shows SEM pictures of pristine and irradiated (at fluence 3×10^{12} ions/cm^2) thin films. The observation of surface topography of irradiated thin film shows micro-bubble formations at the fluence of 3×10^{12} ions/cm^2. These formations of micro-bubbles may be useful in the applications such as MEMS and micro-lens arrays upon further investigations [14,15]. This phenomenon can be understood using a Thermal Spike Model, according to which SHI deposits energy to the material through inelastic collision (electronic energy loss), and with the increase in fluence, the local temperature keeps increasing. At certain fluence, rise in temperature starts causing bubble formations at the surface of the thin film, which is considered as the start of the destruction in the film [16–18]. Thus, the fluence 3×10^{12} ions/cm^2 is the upper limit of SHI irradiation on these films and engineering in properties can be done below this fluence.

3.2. Calculation of energy loss and stopping range

Energy loss of 100 MeV Ag ions within amorphous $As_{40}Se_{60}$ was calculated using SRIM 2008 [19], and the result of the calculation showed that the nuclear energy loss was 9.558 eV/Å and electronic energy loss was 1.4564×10^3 eV/Å. It is clear that the nuclear energy loss is negligible in comparison with electronic energy loss. Hence, SHI deposits energy to the material in the form of electronic energy loss. The calculated stopping range of 100 MeV Ag ions for amorphous thin film sample was 12.66 μm. The magnitude of stopping range was far greater than the thickness of the films (≈ 1 μm). Hence, Ag ions come to the rest in the glass substrate after passing through the thin film.

3.3. Linear optical analysis

The linear optical constants (n, k and α) of thin films were derived using the Swanepoel method from transmission plots [10]. Upper envelope (T_M), lower envelope (T_m) and fringe-free transmission (T_α) were drawn on transmission spectra with the help of Origin 8.0, which are shown in Fig. 4.

Fig. 5 shows a comparison of fringe-free transmissions for pristine and irradiated a-$As_{40}Se_{60}$ thin films. It is clear from the plots that ion irradiation causes reduction in transparency for fluence 3×10^{10} ions/cm^2, and then it increases till fluence 3×10^{12} ion/cm^2. The region of transparency, up to fluence 3×10^{12} ion/cm^2, shifts towards longer wavelength. The observed change in T_α at different fluences is a consequence of structural changes, which can be further understood through Raman measurements.

The determination of discrete values of refractive index at the peak positions was done from transmission spectra using the Swanepoel method. These discrete values were fitted using Cauchy formula (1) with the help of Origin 8.0:

$$n = a + \frac{b}{\lambda^2} \tag{1}$$

where a and b are Cauchy constants. Fig. 6 shows the variation of refractive index with wavelength, where it is observed that the value of refractive index decreases with wavelength. It is the evidence of normal dispersion behavior of the material. SHI irradiation initially increases refractive index value from 2.80 to 3.52 for fluence 3×10^{10} ions/cm^2 and then decreases, as shown in Table 1. This data indicates that the ion irradiation around 3×10^{10} ions/cm^2 is most useful in the case of a-$As_{40}Se_{60}$ compositions if there is a need of additional increase of refractive index.

In present study, the dispersion of the refractive index is described by Wemple–DiDomenico single oscillator relationship [20,21], which is given by

$$n^2(h\nu) = 1 + \frac{E_d E_0}{E_0^2 - (h\nu)^2} \tag{2}$$

This relation is valid only for photon energies lesser than optical bandgap. Linear least square fitting of $1/(n^2-1)$ with

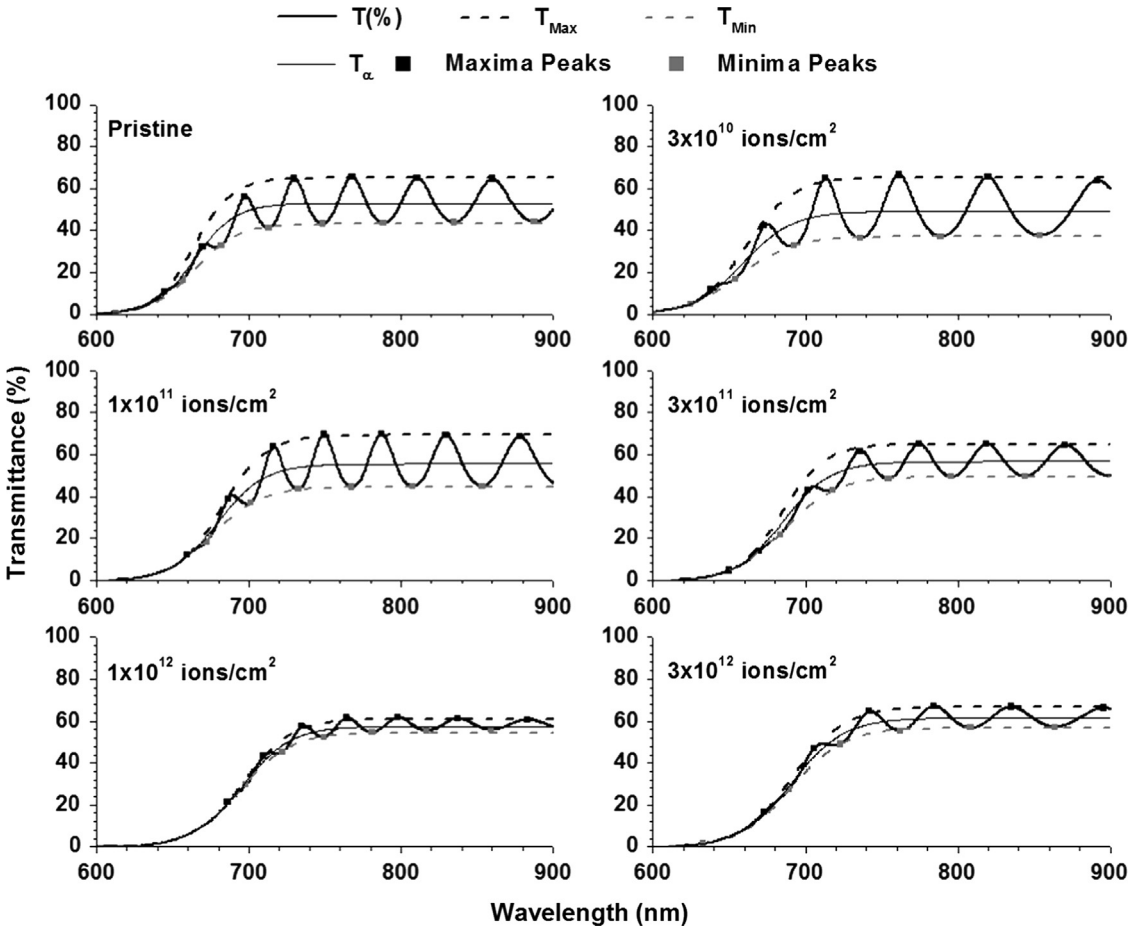

Fig. 4. Transmission spectrum with envelopes for pristine and irradiated thin films.

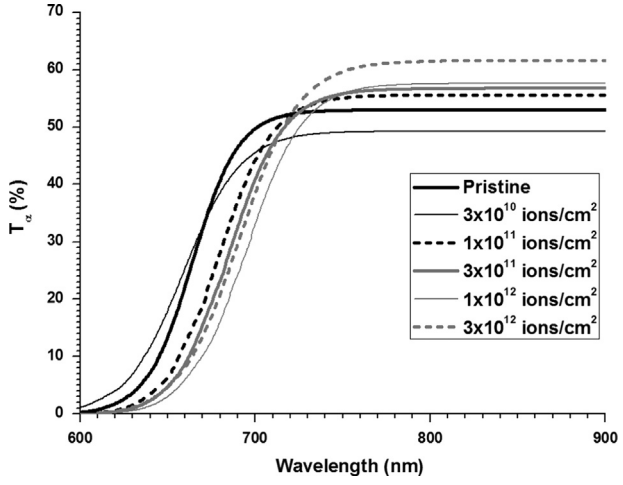

Fig. 5. Fringe free transmission of pristine and irradiated thin films.

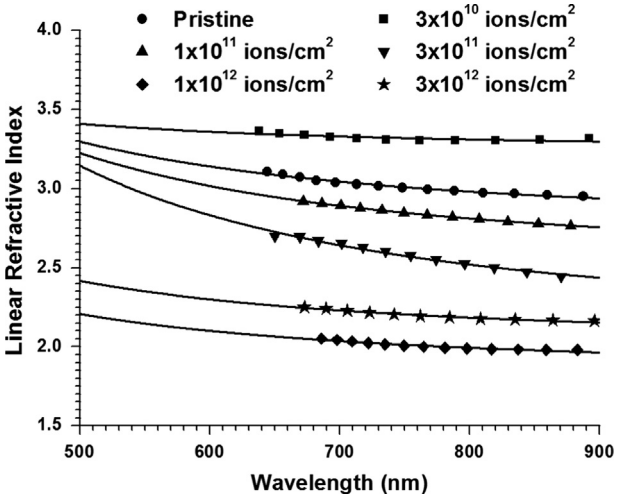

Fig. 6. Plot of refractive index of pristine and irradiated thin films.

$(h\nu)^2$ is obtained using Origin 8.0 as shown in Fig. 7, where the goodness of fit is determined using *R*-Square value, which is ~0.99 for pristine and irradiated films. The values of Dispersive Energy (E_d), Single Oscillator Energy (E_0), and static refractive index (n_0) for pristine and irradiated thin films are determined from WDD plots. Limiting value of first-order susceptibility $\chi^{(1)}$ is determined from n_0 using the following relation:

$$\chi^{(1)} = \frac{(n_0^2 - 1)}{4\pi} \tag{3}$$

Table 1
Linear optical constants of pristine and irradiated a-$As_{40}Se_{60}$ thin films.

	n_0 ($h\nu \to 0$)	$\chi^{(1)}$ ($h\nu \to 0$)	E_d (eV)	E_0 (eV)	E_g (eV)	$B^{1/2}$ (cm^{-1} $eV)^{1/2}$	k (at 775 nm)
Pristine (present study)	2.80	0.547	29.77	4.32	1.76	812.94	0.0062
Pristine (literature)	2.64 [11,29]	0.35 [25]	28.0 [11,29]	4.70 [11,29]	1.76–1.99 [11,29]	861.10–1046.80 [26,27]	0.00866 [28]
3×10^{10} ions/cm^2	3.52	0.762	75.07	7.85	1.74	703.30	0.00822
1×10^{11} ions/cm^2	2.59	0.45	21.3	3.73	1.72	745.05	0.00575
3×10^{11} ions/cm^2	2.22	0.315	12.09	3.05	1.69	718.85	0.00794
1×10^{12} ions/cm^2	1.87	0.200	10.4	3.98	1.66	499.7	0.00585
3×10^{12} ions/cm^2	2.05	0.257	13.25	4.10	1.64	538.64	0.00622

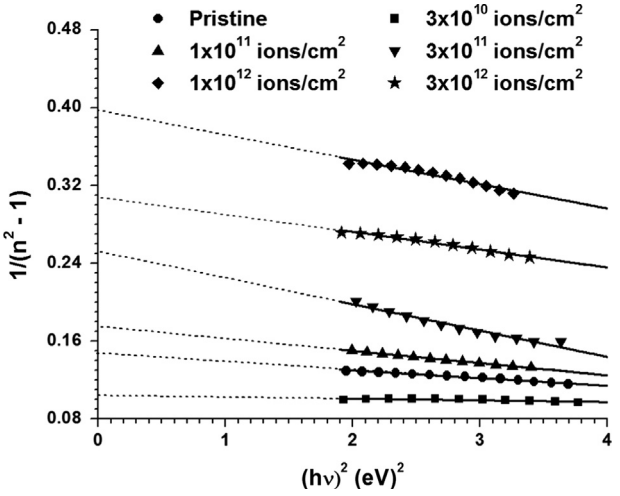

Fig. 7. Linear least square fitting of $1/(n^2-1)$ with $(h\nu)^2$.

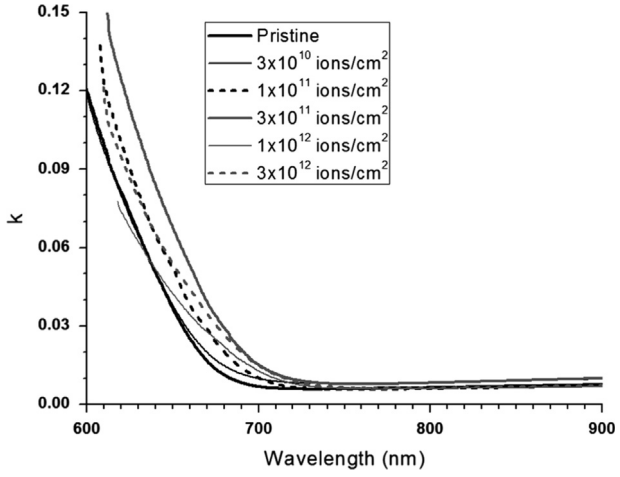

Fig. 8. Plot of extinctions coefficient of pristine and irradiated thin films.

Dispersive Energy (E_d) represents oscillator strength. From Table 1, it is clear that E_d initially increases for fluence 3×10^{10} ions/cm^2, then keeps decreasing up to fluence 1×10^{12} ions/cm^2, and then increases again for fluence 3×10^{12} ions/cm^2. Similar trend is observed for n_0 as both are related to polarizability of the medium. SHI irradiation causes change in coordination number of cation to nearest neighbor anions [22], which changes polarizability of the medium. These coordination defects are responsible for a change in E_d and n_0 upon SHI irradiations. These changes are explained using Raman measurements in the forthcoming section. Values of n_0 in the present study are slightly different from our previously published results [8] for this sample due to the difference in a determination method.

Extinction coefficient (k) represents attenuation of light in a medium. The magnitude of extinction coefficient contains contribution of optical absorption and scattering phenomena. It can be determined using the relation $k = \alpha\lambda/4\pi$, where α is optical absorption coefficient, which can be determined using the Swanepoel method [10]. Fig. 8 shows the variation of extinction coefficient with wavelength. It is clear from this plot that k decreases with wavelength. The reduction of k with wavelength shows that the optical loss reduces with wavelength, which makes it useful optical material in long wavelength region. Table 1 shows the values of k at the wavelength 755 nm for pristine and irradiated thin films. These values demonstrate almost negligible changes in extinction coefficient values upon SHI irradiation, and hence, optical losses of the composition remain almost stable with ion fluence.

Determination of the optical bandgap was done by extrapolating Tauc's plot for indirect bandgap material. Tauc's relation for indirect bandgap material is given as [23]

$$(\alpha h\nu)^{1/2} = B^{1/2}(h\nu - E_g) \tag{4}$$

where $B^{1/2}$ is Tauc parameter and is a measurement of disorder ($B^{1/2}$ α 1/width of localized states, for $\alpha \geq 10^4$ cm^{-1}). Fig. 9 shows Tauc's plots of pristine and irradiated films. It is clear from Fig. 9 and Table 1 that the value of E_g reduces from 1.76 eV to 1.64 eV with SHI irradiation. It is a similar trend as reported in our previous study [8]. In addition, as shown in Table 1, the value of the optical bandgap for pristine sample matches well with the literature. There is a minor difference in numerical values of E_g from our previous study of the same composition. This difference arises due to the evaluation of α using the Swanepoel method in the present study, while the earlier study uses Lambert–Beer's law for the same.

The reduction in optical bandgap upon 100 MeV Ag SHI irradiation is understood on the basis of the Davis–Mott model [24] and cohesive energy (overall bond energy) of the system. SHI irradiation breaks stoichiometric $AsSe_{3/2}$ pyramidal units, which increase local disorder of the system. According to the Davis–Mott model, an increase in disorder increases the width

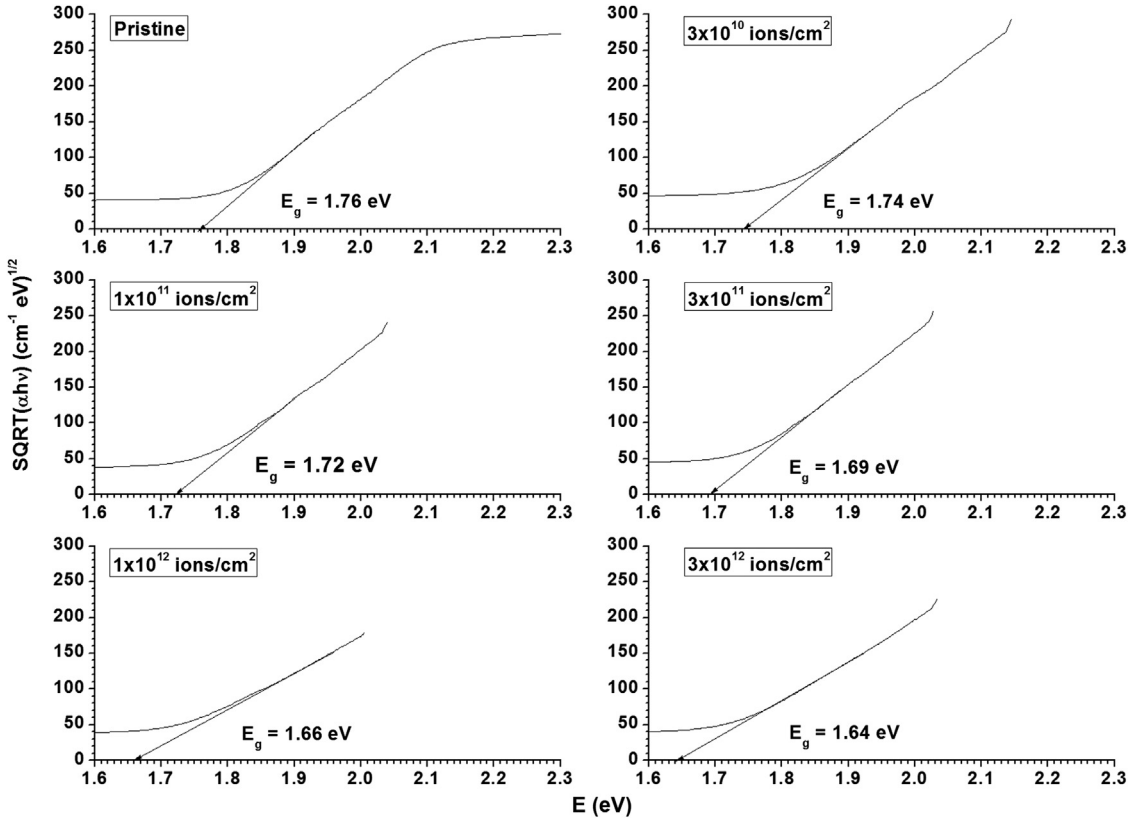

Fig. 9. Tauc's plots of pristine and irradiated thin films.

of localized states in forbidden regions, which is responsible for the reduction in optical bandgap. Increment in the width of localized states with SHI irradiation is supported by the reduction in the value of Tauc parameter ($B^{1/2}$) as shown in Table 1. In addition to that, the reduction in cohesive energy appears due to the conversion of heteropolar As–Se bond into homopolar As–As and Se–Se bonds upon SHI irradiation. This conversion of bonds is supported by Raman measurements explained in the forthcoming section.

3.4. Nonlinear optical analysis

Approximate determination of third-order nonlinear susceptibility $\chi^{(3)}$ in long wavelength region can be determined from generalized Miller's rule, which is given as [12,13]

$$\chi^{(3)} = \frac{A}{(4\pi)^4}(n_0^2 - 1)^4 \tag{5}$$

where $A = 1.7 \times 10^{-10}$ [esu]. The values of $\chi^{(3)}$ shown in Table 2 are compared with the literature value for pristine sample, which shows good agreement. Table 2 shows that the value of $\chi^{(3)}$ initially increases for fluence 3×10^{10} ions/cm^2, then keeps decreasing up to fluence 1×10^{12} ions/cm^2, and then increases again for fluence 3×10^{12} ions/cm^2. Local structural modification may alter polarization of the medium; hence, third order susceptibility may be changed due to ion irradiation, which is shown in Raman measurements.

Table 2
Nonlinear optical constants of pristine and irradiated a-$As_{40}Se_{60}$ thin films in long wavelength limit.

	$\chi^{(3)}$ [10^{-13} esu]	n_2 (Tichy) (10^{-10} esu)
Pristine (present study)	152	1.313
Pristine (literature)	86 [11,29], 25 [25]	1.230 [11,29], 1.220 [25]
3×10^{10} ions/cm^2	573	1.374
1×10^{11} ions/cm^2	72	1.439
3×10^{11} ions/cm^2	16.8	1.544
1×10^{12} ions/cm^2	2.75	1.659
3×10^{12} ions/cm^2	7.4	1.741

The semi-empirical relation that relates optical bandgap (E_g) with nonlinear refractive index is as given by Tichá and Tichý [11]:

$$n_2[\text{esu}] \sim \frac{\overline{A}}{E_g^4} \tag{6}$$

where $\overline{A} = 1.26 \times 10^{-9}$ [esu (eV)^4].

As shown in Table 2, the numerical values obtained using Tichy relation follow a trend of increase in n_2. The obtained values of n_2 of pristine samples match well with the literature, and are far larger than Si based glasses (1.15×10^{-13} [esu]). Hence, selected composition is a better alternative for nonlinear optical applications. In addition, the value of n_2 can be increased using SHI irradiations.

3.5. Raman analysis

Fig. 10 shows Raman plots for pristine and irradiated (3×10^{12} ions/cm^2) thin films. Origin 8.0 is used for multi-peak fitting of Raman spectra to analyze Raman measurements. Raman plot of pristine thin films exhibits three peaks centered at 219 cm^{-1} (Peak 1), 240 cm^{-1} (Peak 2) and 270 cm^{-1} (Peak 3). Peak 1 is assigned as vibration mode of As–As bonds; Peak 2 is the main band of As–Se glasses arises due to $AsSe_{3/2}$ pyramidal units and As_4Se_3 cages. Peak 3 is assigned to vibration mode of Se–Se chains. Though, $As_{40}Se_{60}$ is stoichiometric composition, and according to a chemical bond approach (CBA), hetero-polar As–Se bonds are preferred over homopolar As–As or Se–Se bonds. Hence, in the present composition, it may be expected that all bonds should be As–Se bonds. However, in the present study, the films were prepared using a thermal-evaporation technique, which is responsible for the presence of homopolar As–As and Se–Se bonds in the film. From the Raman spectrum shown in Fig. 10 and Table 3, it is clear that the area under the curve for As–Se bond (0.808) is much larger than the area under the curve for homopolar As–As (0.155) and Se–Se (0.037) bonds. This behavior is apparent in the previous studies of the films prepared using the thermal evaporation technique [30].

Raman plot of thin film irradiated with fluence 3×10^{12} ions/cm^2 also exhibits three peaks at peak positions 223 cm^{-1} (Peak 1), 243 cm^{-1} (Peak 2), and 260 cm^{-1} (Peak 3). It is clear from these plots that SHI irradiation causes change in peak position of the first peak (219–223 cm^{-1}) and the second peak (240–243 cm^{-1}) towards higher wavenumber. A shift towards lower wavenumber is observed for the third peak (270–260 cm^{-1}). Thus, it is clear that SHI irradiation causes shift in peak positions but no new peaks are observed. The absence of the new peaks indicates that no chemical modifications have been made to the film, and changes occurred only in bonding arrangement.

It is clear from Table 3 that the area under the curve corresponding to As–Se bond (Peak 2) reduces from 0.808 to 0.057, whereas the area under the curve for As–As (Peak 1) increases from 0.155 to 0.58, and for Se–Se bonds, it increases from 0.037 to 0.363. Hence, from the above description it is clear that SHI irradiation destructs hetero-polar As–Se bonds into homopolar bonds (As–As and Se–Se bonds). As the energy of As–As bond is 32.1 kcal/mol, As–Se bond is 41.69 kcal/mol, and Se–Se bond is 44 kcal/mol, hence, the cohesive energy of the system before irradiation is 40.29 kcal/mol, and after irradiation it reduces to 36.96 kcal/mol. The reduction in the cohesive energy of the system causes reduction in optical bandgap of thin film sample. Again, the polarizability of the system decreases due to the reduction of As–Se bonds; hence, the linear refractive index, and third-order susceptibility also reduce for fluence 3×10^{12} ions/cm^2.

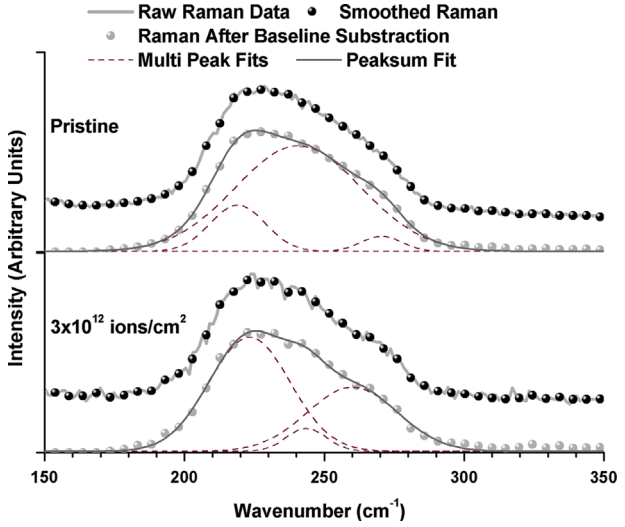

Fig. 10. Raman plots of pristine and irradiated thin films.

4. Conclusion

Irradiation of 100 MeV Ag SHI causes following changes in a-$As_{40}Se_{60}$ thin film:

1. In a-$As_{40}Se_{60}$ thin films, upper limit of ion fluence for engineering in optical properties is below 3×10^{12} ions/cm^2 when the micro-bubble formations start at this fluence as seen in SEM pictures.
2. The optical bandgap (E_g) decreases upon increasing ion fluence. Destruction of $AsSe_{3/2}$ pyramidal units and As_4Se_3 cages increase the number of homopolar bonds, which results in the reduction of the optical bandgap.
3. Maximum increase in linear refractive index and third order susceptibility is achieved for ion fluence 3×10^{10} ions/cm^2. Further increase in ion fluence reduces the values of these parameters.

Table 3
Raman peak details of pristine and irradiated (3×10^{12} ion/cm^2) thin films.

Peak details	Pristine			Irradiated (3×10^{12} ions/cm^2)		
	Peak position (cm^{-1})	Width	Relative area	Peak position (cm^{-1})	Width	Relative area
Peak 1: vibration mode of As–As bonds [31,32]	219	19.54	0.155	223	28.98	0.58
Peak 2: main band of As–Se glasses due to $AsSe_{3/2}$ pyramidal units and As_4Se_3 Cages [33–35]	240	44.83	0.808	243	14.24	0.057
Peak 3: vibration mode of Se–Se bonds in Se–Se chains [36]	270	14.59	0.037	260	32.20	0.363

4. Nonlinear refractive index keeps increasing with increase in ion fluence.
5. The present study is helpful in understanding the threshold limits and tuning of optical/structural properties of a-$As_{40}Se_{60}$ thin films under ion irradiations. The present study can be extended to update the fabrication protocols using ion irradiations upon network glasses for threshold conditions to produce optical components with improved performance.

Acknowledgment

Author is thankful to UGC for providing funds for this work via Minor Research Project: F. no. 8-3 99/2011 (MRP/NRCB), and to IUAC and Dr. D. K. Avasthi (Scientist-H, and IUAC collaborator) for providing required experimental facilities as BTR No. & Activity: 49102 MS.

References

[1] D.K. Avasthi and G.K. Mehta, Springer, Netherlands, 2011.
[2] W. Bolse, B. Schattat, Nucl. Instrum. Methods B 190 (1) (2002) 173–176.
[3] M. Levalois, P. Marie, Nucl. Instrum. Methods B 156 (1) (1999) 64–71.
[4] C. Dufour, A. Audouard, F. Beuneu, J. Dural, J.P. Girard, A. Hairie, M. Levalois, E. Paumier, M. Toulemonde, J. Phys.: Condens. Matter 5 (26) (1993) 4573–4584.
[5] R. Chauhan, A. Tripathi, A.K. Srivastava, K.K. Srivastava, Chalc. Lett. 10 (2) (2013) 63–71.
[6] F. Qiu, T. Narusawa, J. Zheng, Appl. Opt. 50 (2011) 733–737.
[7] B. Luther-Davies, X. Gai, A. Prasad, S. Madden, D.Y. Choi, R. Wang, in: Proceedings of the 35th Australian Conference on Optical Fibre Technology (ACOFT), Melbourne, Australia, IEEE Xplore Digital Library, 2010.
[8] R. Chauhan, A. Tripathi, A.K. Srivastava, K.K. Srivastava, AIP Conf. Proc. 1536 (2013) 599–600.
[9] V. Dimitrov, S. Sakka, J. Appl. Phys. 79 (3) (1996) 1741–1745.
[10] R. Swanepoel, J. Phys. E: Sci. Instrum. 16 (1983) 1214–1222.
[11] H. Tichá, L. Tichý, J. Opt. Adv. Mater. 4 (2) (2002) 381–386.
[12] C.C. Wang, Phys. Rev. B 2 (6) (1970) 2045–2048.
[13] J.J. Wynne, Phys. Rev. 178 (1969) 1295–1303.
[14] R. Maboudian, Surf. Sci. Rep. 30 (6) (1998) 207–269.
[15] J.M. Koo, S.B. Jung, Microsyst. Technol. 13 (11–12) (2007) 1567–1573.
[16] W. Bolse, Surf. Coat. Technol. 158 (2002) 1–7.
[17] F. Seitz, J.S. Koehler, Solid State Phys. 2 (1956) 305–448.
[18] Z.G. Wang, C. Dufour, E. Paumier, M. Toulemonde, J. Phys.: Condens. Matter 6 (1994) 6733–6750.
[19] J.F. Ziegler, SRIM-2008, v. 2008.03. Available from ⟨http://www.srim.org⟩, Last Retrieved on Oct 25, 2013.
[20] S.H. Wemple, M. DiDomenico, Phys. Rev. B 3 (1971) 1338–1351.
[21] S.H. Wemple, Phys. Rev. B 7 (1973) 3767–3777.
[22] A.V. Kolobov, John Wiley & Sons, 2006.
[23] J. Tauc, Plenum Press, New York, 1979.
[24] N.F. Mott and E.A. Davis, Clarendon, Oxford, 1979.
[25] R. Chauhan, A.K. Srivastava, A. Tripathi, K.K. Srivastava, Prog. Nat. Sci.: Mater. Int. 21 (3) (2011) 205–210.
[26] R. Chauhan, A.K. Srivastava, A. Tripathi, M. Mishra, K.K. Srivastava, Proc. SPIE 8173 (2010) (81731C1-81731C10).
[27] L. Tichy, H. Ticha, P. Nagels, R. Callaerts, Mater. Lett. 36 (1998) 294–298.
[28] R. Chauhan, A.K. Srivastava, A. Tripathi, K.K. Srivastava, Prog. Nat. Sci.: Mater. Int. 20 (1) (2010) 54–60.
[29] E.R. Skordeva, J. Opt. Adv. Mater. 1 (1) (1999) 43–47.
[30] P. Němec, J. Jedelský, M. Frumar, M. Štábl, M. Vlček, J. Phys. Chem. Solids 65 (7) (2004) 1253–1258.
[31] M. Frumar, Z. Polák, Z. Černošek, J. Non-Cryst. Solids 256–257 (1999) 105–110.
[32] R. Ston, M. Vlcek, H. Jain, J. Non-Cryst. Solids 326–327 (2003) 220–225.
[33] V.Q. Nguyen, J.S. Sanghera, J.A. Freitas, I.D. Aggarwal, I.K. Lloyd, J. Non-Cryst. Solids 248 (1999) 103–114.
[34] K. Saitoh, O. Uemura, T. Usuki, Y. Kameda, J. Non-Cryst. Solids 192–193 (1995) 286–291.
[35] G. Lucovsky, Springer, Berlin, 1979.
[36] P. Tronc, M. Bensoussan, A. Brenac, C. Sebenne, Phys. Rev. B 8 (12) (1973) 5947–5956.